




Wildfire activity enhanced during phases of maximum orbital eccentricity and precessional forcing in the Early Jurassic

Teuntje P. Hollaar^{1,2}[✉], Sarah J. Baker¹, Stephen P. Hesselbo^{2,3}, Jean-François Deconinck⁴, Luke Mander⁵, Micha Ruhl⁶ & Claire M. Belcher¹

Fire regimes are changing due to both anthropogenic climatic drivers and vegetation management challenges, making it difficult to determine how climate alone might influence wildfire activity. Earth has been subject to natural-background climate variability throughout its past due to variations in Earth's orbital parameters (Milkankovitch cycles), which provides an opportunity to assess climate-only driven variations in wildfire. Here we present a 350,000 yr long record of fossil charcoal from mid-latitude (~35°N) Jurassic sedimentary rocks. These results are coupled to estimates of variations in the hydrological cycle using clay mineral, palynofacies and elemental analyses, and lithological and biogeochemical signatures. We show that fire activity strongly increased during extreme seasonal contrast (monsoonal climate), which has been linked to maximal precessional forcing (boreal summer in perihelion) (21,000 yr cycles), and we hypothesize that long eccentricity modulation further enhances precession-forced fire activity.

¹WildFIRE Lab, Global Systems Institute, University of Exeter, Exeter, UK. ²Camborne School of Mines, University of Exeter, Penryn Campus, Penryn, UK. ³Environment and Sustainability Institute, University of Exeter, Penryn Campus, Penryn, UK. ⁴Biogéosciences, Université de Bourgogne/Franche-Comté, Dijon, France. ⁵Department of Environment, Earth and Ecosystems, The Open University, Milton Keynes, UK. ⁶Department of Geology, Trinity College Dublin, The University of Dublin, Dublin, Ireland. ✉email: t.p.hollaar@exeter.ac.uk

Earth is currently experiencing rapid climatic change due to anthropogenic carbon emissions since the industrial revolution¹ and this in turn, appears to be contributing to variations in wildfire activity across many regions of the globe². However, it is difficult to disentangle natural wildfire climate-drivers from anthropogenic influences on ignitions³, human-driven shifts in distribution of vegetation types across the landscape⁴, or fuel management practices⁵. This makes the study of palaeofire of utility in disentangling the role of land management practices^{4,5} from climate change alone in driving variations in wildfire activity. Natural forcings (such as Milankovitch cycles) act to influence climate variations⁶, have done so throughout Earth's long past^{7,8}, and provide an excellent framework to study how regular background climatic shifts can influence fire activity.

Milankovitch theory describes how Earth's orbital motions of precession, obliquity and eccentricity determine the seasonal and latitudinal distribution of insolation received on Earth and, to a smaller extent, the net received solar radiation^{9,10}. These orbital processes cause variations in average regional and global temperatures and ice sheet growth (e.g. forcing the Pleistocene glacial cycles), seasonality, monsoonal strength, and associated storm activity^{11–13}. All of these factors feed back into determining vegetation type and abundance as well as weathering and runoff from the land to the ocean, ocean mixing, productivity and marine and terrestrial carbon burial^{14–18}.

Orbital processes operate at multiple timescales, in the present day from ~21,000 years (precession), ~40,000 years (obliquity), ~100,000 years (short eccentricity) and ~405,000 years (long eccentricity), as well as longer period amplitude modulations^{19–21}. As an example, currently the Earth is in aphelion on the 4th of July (leading to a relatively cool summer in the northern hemisphere), with the Earth's orbit also close to lowest eccentricity (minimum)^{22,23}. In other words, the current, near circular shape of the Earth's orbit should result in smaller seasonal extremes that provide a weaker summer monsoon and milder winters. Over the next ~50,000 years Earth will gradually move into an eccentricity maximum, hence seasonal differences and monsoonal climates will amplify in both hemispheres according to precessional phase²⁴.

Orbital cycles have been shown to influence wildfire activity as evidenced by assessment of variations in the abundance of fossil charcoal^{25–31}, which is understood to provide a proxy for wildfire activity in Earth's past³². For example, orbitally driven wildfire activity has been inferred for the Middle Pleistocene to Holocene from sites in southern Africa that show increased charcoal (fire activity) over a precessional cycle, driven by amplification of the African monsoon²⁷. Here, the increased amount of monsoonal rainfall, during maximal precessional forcing (austral summer coincides with perihelion), likely seasonally enhanced the vegetation abundance (fuel) in flammable grasslands in an otherwise dry climate, thus promoting fire activity²⁷. Similarly, Hao et al.³³ also found variations in fire activity, evidenced by both charcoal and soot deposition over a single precessional cycle preserved in Holocene aged sediments of Quighai Lake in China. Other studies have assessed records of charcoal and black-carbon over long stretches of Quaternary time^{25,26,28,30,31,34–36} and have suggested variations in fire activity linked to marine isotope stages, which are driven by orbital cycles. Kappenberg et al.³⁵ found evidence for enhanced fire during periods of warm/humid climatic conditions that they linked to the influence of short eccentricity (100,000 year cycles) on shifts in vegetation type. Hence, although the importance of orbital forcing on Earth's climate and the environment is well recognized, an understanding of its impact on wildfire activity is predominantly limited to the Quaternary record.

Long-term, deep-time trends in orbitally driven climate cycles and their influence on wildfire activity during periods of global

warmth are understudied. Recently Zhang et al.²⁹ suggested the presence of variations in the ratio of the coal macerals vitrinite:inertinite in the Middle Jurassic coals of the Yan'an Formation of China, where inertinite is considered to be fossil charcoal preserved in coal³⁷. Increased amounts of inertinite are observed to vary with a periodicity that occurs on average every 0.9 m through the coal succession. This cycle has been suggested to represent orbital precession on the assumption that average coal accumulation rates of published studies apply to the fossil coal successions in the Ordos Basin (China)²⁹. Despite the hint of a 21 kyr orbital forcing on wildfires affecting ancient mires, the age model for these coal seams has not been astrochronologically tuned, making it difficult to assess the true drivers of this apparent cyclicity. There remains to our knowledge no study that assesses climate-wildfire relationships over the long stretches of Earth's history required to get near to capturing the influence of the long eccentricity orbital cycle.

Orbitally paced deposition of marine sediments in the Early Jurassic (201.4–174.1 Ma) of the UK is well documented^{14,16,38–44}, and a high-resolution astrochronological age model already exists for the marine Pliensbachian (~192.5–183.8 Ma) in the Llanbedr (Mochras Farm) borehole (Fig. 1, Supplementary Figs. 1, 2)^{43,45,46}. This location in the Cardigan Bay Basin (west Wales), with an Early Jurassic mid-palaeolatitude of ~35°N (Fig. 1) exhibits multiple lithological couplets of: 1) clay and organic-matter enriched dark grey calcareous mudstone, and; 2) carbonate-rich, pale grey mudstone (Fig. 1)^{43,46}. Changes in lithology and elemental concentrations within this sedimentary record have been shown to occur at the astronomical (Milankovitch) periodicities of ~21, ~100 and ~405 kyr, reflecting precession and short and long eccentricity^{43,45}. The presence of these short and long eccentricity cycles are supported by an independent analysis of the carbon isotope ($\delta^{13}\text{C}_{\text{org}}$) record that exhibits a similar cyclicity⁴⁶ (Supplementary Fig. 2), and via a range of power spectral analyses of the Ca time series data, including a discussion of the red noise models used⁴⁵. The latter study confirmed that a 2π resolution MultiTaper Method power spectral analysis resolves a 6 m cycle (expression of 100 kyr eccentricity in accordance with the GTS2012⁴⁷) above the 99% confidence limit⁴⁵.

Here we present a high-resolution and astrochronologically tuned record of wildfire activity that focuses on an interval of the Mochras succession that most clearly shows the expression of precession and eccentricity^{43,45,46} (Fig. 1), and which allows us to examine the link between wildfire and climatic shifts. This interval also lacks any large perturbations in $\delta^{13}\text{C}_{\text{org}}$ (and thus disruptions to the global carbon cycle) that would have been related to non-Milankovitch forcing (Supplementary Fig. 2 grey band), hence we ascertain that any periodic variability in charcoal (and thus wildfires) are linked to orbital forcing. Charcoal data were obtained from >139 samples taken from ~17 m of the Upper Pliensbachian Margaritatus Zone (Supplementary Fig. 1), where they were sampled at an approximate 2000 year temporal resolution (ref. 43; Fig. 1). The section studied represents ~350,000 years and sits within part of the long-eccentricity cycle number 459 ± 1 (Supplementary Figs. 1, 2)^{10,47,48}. We present counts of 46,204 macrocharcoal particles (>125 μm) and counted projections of >15 million microcharcoal particles (<125 μm) which are coupled to X-ray diffraction (XRD) analysis of clay mineral ratios and XRF elemental analyses at the same sample resolution.

In the present day, the nature of the clay minerals formed in soils depends on the intensity of the weathering processes and in particular on hydrolysis which itself depends on precipitation, temperature, humidity and erosion related to runoff⁴⁹. For example, smectite forms preferentially in a warm climate with contrasting seasonal humidity, while kaolinite forms in a regularly warm and humid climate determining a high intensity of hydrolysis^{50–52}. Hence, coupling of clay mineral ratios in the

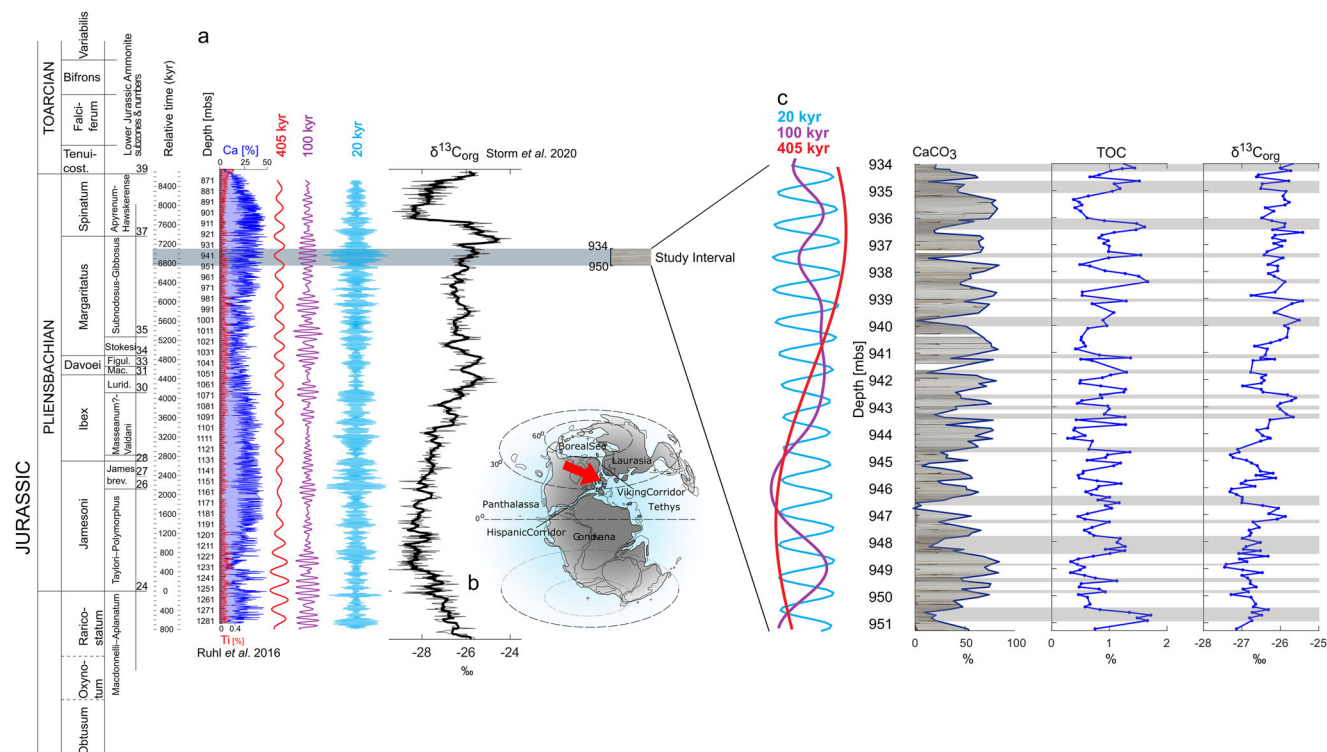


Fig. 1 Stratigraphic context of the Mochras borehole in the Upper Pliensbachian (934–951 mbs), Margaritatus Zone, Subnodosus-Gibbosus subzones. **a** The Mochras borehole has been cyclostratigraphical tuned based on two independent geochemical time series, elemental Ca record^{43,45} and $\delta^{13}\text{C}_{\text{org}}$ ⁴⁶. The sampled interval for this study shows strong orbital forcing⁴³ and is within the stable part of the $\delta^{13}\text{C}_{\text{org}}$ record⁴⁶, allowing examination of climatic background fluctuations and the effects of Milankovitch cycles on the charcoal record. **b** The Mochras borehole was located at a palaeo-latitude of $\sim 35^\circ\text{N}$ ⁸⁵, within the Laurasian Seaway^{86,87} south of the Viking Corridor that linked the NW Tethys Ocean to the Boreal Sea⁸⁸. Reprinted from ref. ⁴³. Copyright (2021) with permission from Elsevier. **c** Detail of the filtered orbital periodicities in the Pliensbachian carbonate record⁴³ are plotted next to data from this study, and span approximately 350 kyr^{43,45}. Clear alternations of carbonate-rich and TOC-enhanced lithological couplets are observed at a metre scale, which are forced by precession⁴³. Finally, high resolution $\delta^{13}\text{C}_{\text{org}}$ data confirms that the 934–951 mbs interval contains only a minor swing of $\sim 0.5\%$.

studied samples, with estimated changes in wildfire activity enables linkages to be made between variations in wildfire and the regional hydrological cycle in our studied section. We further present a palynofacies analysis in order to provide information on the source of the constituent marine and terrestrial organic matter particles⁵³. This allows for inferences on the influence of shifting temporal and spatial variations in rainfall patterns on vegetation (the fuel for wildfires), and assessment of the potential for preservational changes of the organic matter particles, or shifts in runoff intensity, that might otherwise bias the wildfire and vegetation signal. In addition, we report the total organic carbon (TOC) and carbonate content, and the bulk organic carbon isotopic composition ($\delta^{13}\text{C}_{\text{org}}$) of the studied samples, to further assess whether non-orbital climatic changes could be responsible for variations in inferred fire and hydrology. Our aim is to test the hypothesis that orbitally driven shifts in the hydrological cycle regulate wildfire activity in a pre-anthropogenic world, indicating that relatively low-level background changes in climate alone have been able to influence wildfire activity. We show that charcoal abundances and inferred wildfire activity naturally fluctuate substantially on short (precession) and long (one near complete 405-kyr eccentricity cycle) time scales, and particularly during inferred maximum eccentricity when precession cycles are most strongly expressed.

Results and discussion

The studied section has alternating carbonate-rich and TOC-enhanced lithological couplets, with a high abundance of carbonate

present throughout, and so the apparent abundance of charcoal particles could be influenced not only by variations in terrestrial influx but also by carbonate dilution. In order to account for the latter possibility, charcoal abundances have been normalized by the $(\text{Si}+\text{Ti}+\text{Al}+\text{Fe})_{\text{XRF}}/\text{Ca}_{\text{XRF}}$ ratio (Supplementary Fig. 3), following a similar approach used by Daniau et al.²⁷.

Evidence for variations in wildfire driven by long-term changes in the hydrological cycle. Our analyses reveal a major shift in both macro- and micro-fossil charcoal abundance within the studied Pliensbachian (Margaritatus Zone) section from 934–951 mbs (metres below surface) (Fig. 2). Low charcoal abundance is observed between 951 and 944 mbs, followed by an interval between 944 and 934 mbs of high charcoal abundance. This upper part shows a mean four-fold greater abundance of macrocharcoal and a two-fold increase in microcharcoal. This substantial increase in charcoal abundance starting at 944 mbs does not correspond to any major change in lithology or to any large variation in the abundance of terrestrial phytoclasts (Fig. 2), with the latter accounting for on average $\sim 28\%$ of the total terrestrial organic particles throughout the studied section. The observations imply that this major shift in charcoal abundances is a true signal of wildfire rather than of major facies change or preservational artefact.

A similar pattern is apparent in our chemical analyses, where mean CaCO_3 content for the lower part of the section is 54% and rises to a mean of 61.5% in the upper part (Figs. 1 and 2); mean TOC is 0.81% in the lower section and 0.91% in the upper section (Fig. 1); for carbon isotopes, average $\delta^{13}\text{C}_{\text{org}}$ becomes very slightly

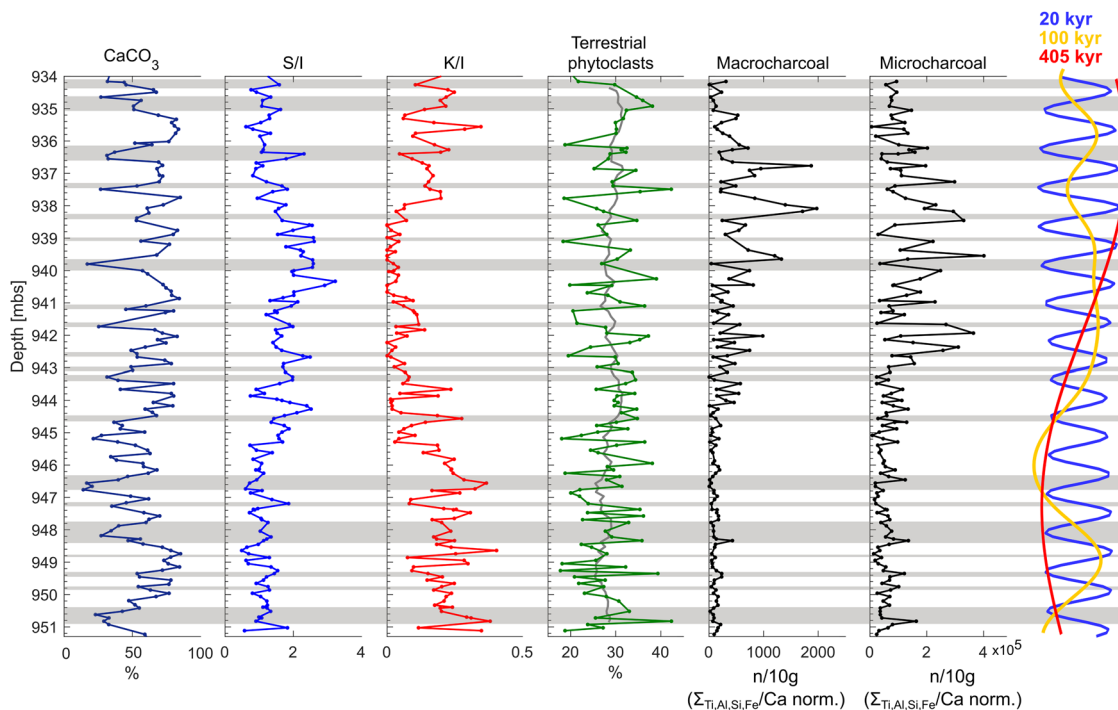


Fig. 2 Short and long cyclic alternations are observed in the proxy records during the studied interval. A major shift at ~944 mbs is observed in the calcium-carbonate, smectite/illite, kaolinite/illite, percentage of terrestrial organic particles and the macro- and micro-charcoal abundance. The moving average (~1 m) of the percentage terrestrial phytoclasts is displayed in the light grey curve. TOC-enhanced lithological beds are marked by a light grey bar, with the carbonate-rich layers displayed in white. In the part of the record where there is evidence for strong seasonality (i.e. S/I-rich) the expression of precession is visible in large macrocharcoal peaks, which are coeval with carbonate-rich beds. We hypothesize that this interval (~934–944 mbs) lies within an increasing phase of a long eccentricity cycle. The orbital filters are derived from the elemental Ca record of Ruhl et al.⁴³ spanning the Margaritatus Zone of the Pliensbachian of Mochras.

more positive, shifting from a mean of -26.7% (V-PDB) to a mean of -26.1% (V-PDB) (Fig. 1). More notably, the ratio of smectite/illite (S/I) increases in the upper part of the section from a mean of 1.2 to a mean of 1.7, whilst the kaolinite/illite (K/I) ratio shifts from a mean of 0.2 to 0.9 (Fig. 2). All shifts in the $\delta^{13}\text{C}_{\text{org}}$ are below $\sim 0.6\%$, and therefore no major changes in the global carbon cycle have been inferred for the studied time interval⁴⁶. Thus, major internal Earth-system-forced global climatic upheavals are unlikely to explain the inferred large shift in fire activity and other environmental proxies. However, the study interval spans the minimum and maximum parts of long eccentricity cycle number 459 ± 1 (Supplementary Fig. 2, cf.^{10,47,48}), one of a series of such cycles based on previously published cyclostratigraphic studies of the same core derived from visual analysis, and Ca and $\delta^{13}\text{C}_{\text{org}}$ time series data (Supplementary Figs. 1 and 2)^{43,46}. Although this major shift in charcoal abundance occurs within a long eccentricity cycle (Fig. 2), our record does not span sufficient time to robustly test that fire activity in this record is modulated by that cycle. However, our analysis does indicate a major shift in the hydrological cycle throughout the studied section consistent with such an interpretation.

Clay mineral abundances are used to reconstruct physical erosion and weathering, and detrital clays fluctuate in abundance due to changes in the hydrological cycle^{49,50}. In the Pliensbachian of the Cardigan Bay Basin, smectite is found to be detrital and therefore reflects a warm, seasonally-wet climate⁴⁹. Next to this, detrital kaolinite is formed under a year-long wet, hot climate^{50,51}. Based on the changes of smectite and kaolinite abundance we interpret a change in seasonality, where our clay analyses show that towards the top of the lower part of the studied succession (~945–944 mbs) the proportion of K/I starts to

decrease whilst S/I starts to increase, reaching minimum K/I and maximum S/I values half way into the upper section (~940 mbs) (Fig. 2). In accord with other Mesozoic examples^{18,46,54} we take this to be evidence of a switch to a seasonally dry climate at this time which affected the predominant clay mineral species formed in the contemporaneous soils^{50,51}. The anti-correlation of smectite and kaolinite in this study further supports the idea that the smectite is derived from pedogenic profiles formed under a temperate and seasonally humid climate^{49,52,55,56}. In the present study, an increase in carbonate is observed simultaneously with enhancement of detrital soil-formed smectite (934–944 mbs, Fig. 2). This coupling is in good agreement with the long-term Pliensbachian clay mineral record from Mochras⁴⁹, where an increase in the proportion of S/I corresponds to carbonate-rich intervals and the relative abundance of K/I rises coevally with organic carbon-rich deposits (Supplementary Fig. 3). This suggests that the lower part of the studied section between 951 and 944 mbs records a moist climate regime of low seasonality and that the upper part of the section between 934 and 944 mbs records a climate regime in which strong seasonality occurred commonly (Figs. 2 and 3).

The nature of fuels, both plant type and moisture status, strongly influence ignition and fire behaviour^{57,58,59}. These factors tend to follow seasonal trends in the modern day and are driven by the balance of temperature and precipitation, which determines relative humidity, and amount and type of vegetation, as well as its moisture content. Vegetation (fuel) types would not have been the same as today, because neither flowering plants nor grasses had evolved in the Jurassic. A study of the organic walled phytoplankton from the Mochras core noted the presence of some terrestrial sporomorphs⁶⁰ and found that the pollen grain *Classopollis* spp. dominates the pollen assemblages, whilst spore

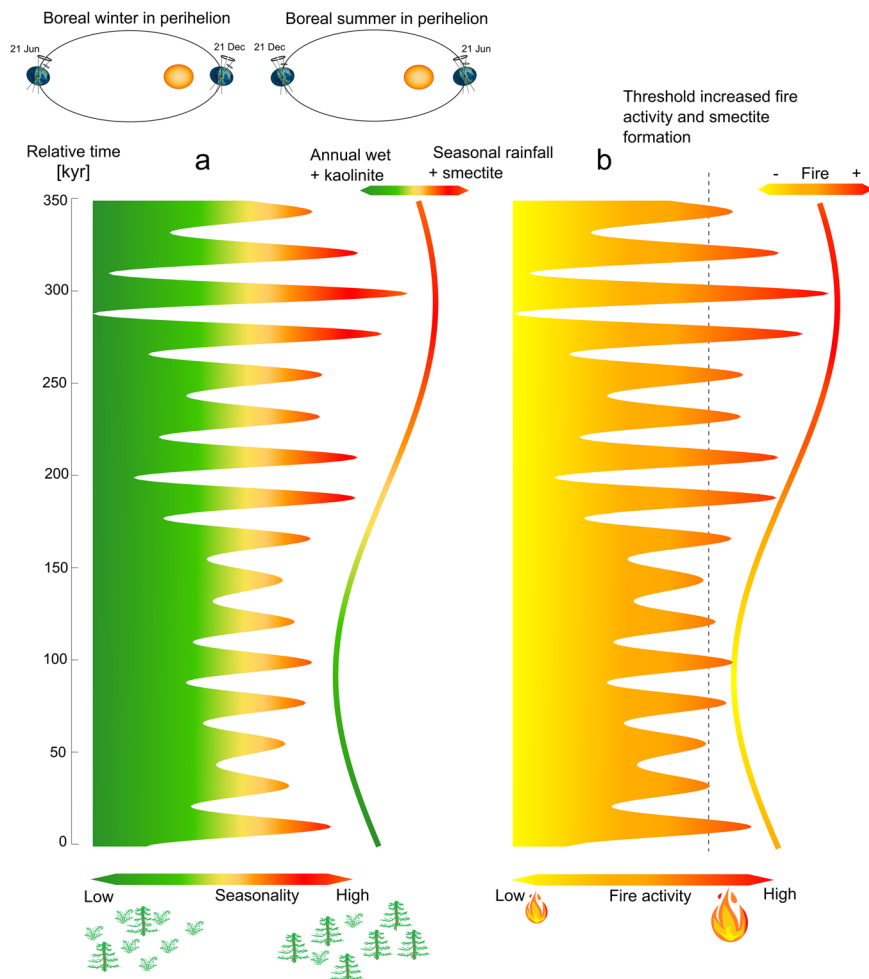


Fig. 3 Schematic model of eccentricity modulated, precession driven changes in seasonality and wildfire over the studied interval. a Magnitude changes in seasonality are plotted on the x-axis over relative time (kyr) on the y-axis. One precession cycle contains ~10 kyr of relatively high seasonality (red) and ~10 kyr of relatively weaker seasonality (green) (for the Northern Hemisphere). Strongest seasonality is found during maximal precessional forcing (hemisphere specific summer coinciding with perihelion), coinciding with maximum 405 kyr eccentricity. The 405 kyr eccentricity modulation is schematically drawn in the green to red curve, with higher amounts of kaolinite indicating a year-round wet season and an acceleration of the hydrological cycle, whereas enhanced amounts of smectite indicate the presence of a dry and wet season (monsoonal climate). Coupled to a change in the hydrological cycle, we hypothesize that vegetation shifted from humidity loving species to flora that thrived in a seasonally dry climate. **b** Magnitude changes in wildfire activity are plotted on the x-axis and relative time (kyr) on the y-axis, with low fire activity on the left (yellow) to high fire activity on the right (red). Coeval with changes in seasonality, fire activity changes over each precession cycle, which contains ~10 kyr of relatively high wildfire activity (and seasonality) and ~10 kyr of relatively low wildfire activity (and seasonality). Next to this, wildfire activity is influenced by the 405 kyr modulation. The dashed black line indicates a fire threshold, after which the seasonal contrast is likely extreme enough to lead to enhanced charcoal and smectite in the fossil record.

abundance is generally low. *Classopollis* pollen, which derive from a now extinct group of conifers⁶¹, the cheirolepidaceans, constitute a substantial to dominant proportion of the total pollen observed (30–95%) in the Margaritatus Zone of the Mochras core⁶⁰. Hence, the forest floors on the emergent land surfaces around the Cardigan Bay Basin, in which the Mochras sedimentary archive was deposited, were likely needle-litter dominated, and would have supported an understory of ferns, tree ferns and cycads⁶². The temperate climate zone in which the Cardigan Bay Basin was situated at this time^{63,64} likely favoured the presence of such an understory during wet phases; both throughout the prolonged annual-humid climate (K/I enhanced interval) and during the seasonal (monsoonal) wet phases of the seasonal-arid climate (the S/I dominated interval).

These changes in seasonality over multi-100-kyr timescales, have been linked to eccentricity forcing in the Jurassic, which by modulation of precession forcing, regulates monsoonal strength and

hence runoff^{41,43,46,65}. Eccentricity pacing of pollen to spore ratios has been interpreted for the End Triassic/Early Jurassic from the neighbouring Bristol Channel Basin, with increased relative abundance of pollen linked to an intensified monsoon⁶⁵. It has been suggested that the expansion of humid and semi-arid climate zones to higher latitudes⁶⁶ during eccentricity maxima caused precipitation to penetrate further into the hinterland of this region⁶⁵. This interpretation posits an expansion of dry-adapted vegetation such as cheirolepidacean conifers into larger areas in the hinterland of the Bristol Channel Basin during eccentricity maxima⁶⁵. Hence the shift we observe in moisture regime (e.g. clay data) at Mochras could similarly be linked to the orbital cycle of eccentricity and the shifts in vegetation and flammability in the surrounding landmasses of the Cardigan Bay Basin.

Conifers have biochemical and morphological traits that make them particularly flammable whether dry or live^{58,67}. Ferns are known to be flammable when fully cured (dry) and, indeed,

high dry-fern fuel loads can carry intense fires⁵⁸. However, four out of five species of live/fresh moisture ferns were found not to be ignitable in tests⁵⁸, whilst all seven species of conifer tested ignited even when live and moist. Hence, the lack of a dry phase, which is indicated by our clay record to occur in the K/I rich interval, would likely have prevented frequent ignition in either moist fern-dominated understories, or made it less likely in those dominated by fully wet needle litter. In contrast, the expansion of dry-adapted conifers (enhanced fuel load) in the proposed monsoonal phase (S/I rich interval) would have enhanced the abundance of easily ignitable vegetation⁵⁸. Thus, during the year-long-wet climate (high K/I), fuel is hypothesised to have been sufficiently abundant to support fires, but fuel moisture levels likely rarely fell below the threshold for frequent ignition and fire spread. During the strong seasonal climate (high S/I), in contrast, a short wet season would have allowed for rapid increase in vegetation biomass (fuel), both in conifers and/or ferns, but critically over the much longer dry season these fuels would have become more easily ignitable and more capable of carrying intense spreading fires. Therefore, we conclude that irrespective of changes to vegetation type and amount (i.e. increased fuel load) fire activity in the region of the Cardigan Bay Basin increased due to climatically driven effects on fuel load and its moisture content.

Precession driven variations in wildfires. Superimposed on the broad shift from lower to higher fire activity discussed above, are also relatively rhythmic fluctuations in the abundance of both micro- and macro-charcoal, clay minerals, and terrestrial phytoclasts (Fig. 2). Periodic changes in TOC and Ca in the studied Early Jurassic (Pliensbachian) succession, and associated alternations between darker grey mudstones and paler grey marls/limestones occur every ~1 m. The astrochronologically tuned timescale for the whole Pliensbachian part of the Mochras core of Ruhl et al.⁴³ indicates that a precessional forcing is reflected in the deposition of these lithological couplets of carbonate-rich (organic-poor) and more organic-enriched (carbonate-poor) beds, with the magnitude of variability further modulated by short and long eccentricity forcing. Whilst, we have accounted for organic and carbonate dilution in our charcoal records (Supplementary Fig. 4), peaks in charcoal abundance generally appear to occur in the carbonate-rich part of precession modulated lithological couplets (Fig. 2). For example, this can be seen in the large

peaks in the macrocharcoal record between 935 and 940 mbs; these peaks are similarly pronounced in the microcharcoal record. The palynological fraction in this interval shows minor (~28%) fluctuations in the relative abundance of terrestrial organic particles vs marine organic particles (Fig. 2), without any correlation to TOC ($r = -0.03$) or carbonate concentration ($r = 0.02$) (Supplementary Fig. 5a and b), implying that the source of the organic particles does not vary with the lithological alternations on a bedding-scale (i.e. is not a taphonomic artefact). We found no correlation ($r = 0.02$) for macrocharcoal and very weak positive correlation ($r = 0.27$) in microcharcoal (Pearson correlation) (Supplementary Fig. 5c and d) between the charcoal content and the relative abundance of terrestrial compared to marine organic matter particles through the studied section. This hints that there may be additional factors influencing the microcharcoal abundance, such that the microcharcoal record provides a less reliable record of fire activity in this case.

The previously established astrochronological time-scale for the studied sedimentary succession⁴³ allows for our wildfire and clay data to be analysed in the time-domain (with the new data tuned to the 100 kyr eccentricity cycle derived from the elemental Ca record; Fig. 1, Supplementary Fig. 1). Power spectrum analysis for the data in the time domain shows: (1) Ca, TOC and illite peaks at 99% confidence, with a periodicity of ~40.5–29.5, ~27.4–21.8, ~18.5, ~17–14 kyr (Supplementary Fig. 6) (we found no relationship between kaolinite/illite or smectite/illite ratios at any of these periodicities); (2) macrocharcoal abundance peaks at over 99% confidence, with a periodicity of ~46–29.7 kyr and ~20.3–17.6 kyr (Fig. 4); (3) the percentage of terrestrial phytoclasts also appear to peak at periodicities of ~50 kyr and ~28–23.9 kyr at 95% significance and at a periodicity of 19.7–17.4 kyr at 99% significance (although these do not obviously correlate with lithological changes (Fig. 2, Supplementary Fig. 5 and 6)), and; (4) there is no similar periodicity in the microcharcoal record (Supplementary Fig. 6), likely because the signal has been interfered with owing to the addition of terrestrial influx, as evidenced by the weak but positive correlation between microcharcoal and the relative abundance of terrestrial material (e.g. $r = 0.27$).

In the Jurassic, precession cycles had periodicities that averaged around ~20 kyr and obliquity cycles that averaged around ~35 kyr^{10,68,69}. The new 100 kyr eccentricity tuned data in the time

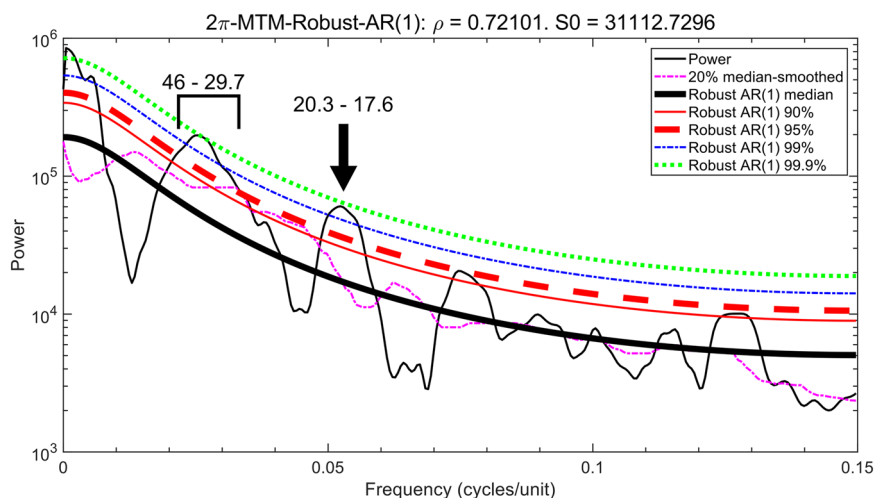


Fig. 4 Multi-taper (MTM; 2π) power spectrum of the macrocharcoal record ($(\text{Si}+\text{Ti}+\text{Al}+\text{Fe})_{\text{XRF}}/\text{Ca}_{\text{XRF}}$ normalized) in time domain. This power spectrum was obtained in the Acycle software, with robust red noise models¹⁰⁰. Dominant peaks are shown at the obliquity (~46–29.7 kyr) and precession (~20.3–17.6 kyr) frequency bands at 99% significance. The macrocharcoal record was tuned to the 100 kyr eccentricity of the elemental Ca record spanning the Margaritatus zone (see Supplementary Fig. 1). The Ca record is derived from Ruhl et al.⁴³.

domain appears to show strong evidence for precession-controlled higher frequency fluctuations in palaeoclimatic and environmental change, and associated fluctuations in wildfire (macrocharcoal) (Figs. 2 and 4; Supplementary Fig. 6).

In the upper part of the section, macrocharcoal abundance varies between as much as 3 and 1973 particles per 10 g of sediment (normalized) over ~20 kyr precessional scale cycles, whilst microcharcoal ranges between $\sim 5.8 \times 10^3$ and $\sim 4 \times 10^5$ particles per 10 g of sediment (normalized), although our analysis did not show a regular alternation on a precessional timescale in the microcharcoal. The smectite/illite ratio varies between 0.6 and 3.2 over individual precession cycles throughout the upper part of the section; this in contrast to a variation between 0.5 and 2.5 in the lower part. This hints at more extreme (climatic) contrasts attributable to eccentricity modulation of precession in the upper part (Figs. 2 and 3).

The origin of the fine-grained carbonate in precessional couplets is likely derived from planktonic organisms and/or localised periplatform ooze, albeit with considerable recrystallisation (e.g. Ref. 14). Carbonate production is facilitated in warm shallow seawater^{70,71} with low dilution by terrigenous sediment^{71,72}. These factors will have been influenced by precessional insolation changes that altered the monsoonal strength. A seasonal (monsoonal) climate would have influenced riverine flow, carrying clay and nutrients from the terrestrial to the marine realm during the wet-season. Subsequently this process would have led to increased productivity in the marine waters which, together with increased terrestrial runoff and potential density stratification, could have led to low oxygen levels in the bottom water¹⁴. This would have been followed by a phase of increased aridity diminishing the overall flux of clay and nutrients from land to the marine surface waters, leading to fine biogenic carbonate dominating the deposited sediment¹⁴. Thus, carbonate-enriched sedimentation in the Cardigan Bay Basin possibly corresponded to maximal precessional forcing (boreal summer in perihelion), where a strong monsoon led to strong seasonality and a prolonged dry period. These carbonate-rich beds, which host the greatest charcoal content, are therefore likely linked to a strongly seasonal climate and a monsoonal system. It is likely that eccentricity modulation of the precession signal was further enhanced due to the position of the continental plates either side of an equatorial Tethys ocean during this period of Earth history, which enabled the existence of a so called 'megamonsoon'^{73–78}.

Peaks in illite abundance also correlate to these carbonate-rich beds (Supplementary Fig. 7). A rise in illite, relative to kaolinite and smectite, signifies a higher degree of physical erosion relative to chemical weathering⁴⁹. Erosion of poorly evolved soil profiles led to lower nutrient supply to the basin. This scenario is favourable for calcifying organisms, because organic phytoplankton blooms during high nutrient conditions would otherwise have outcompeted the calcifying organisms for substrate⁷⁹. Such an increase in physical erosion can be expected during intense monsoonal rainfall^{80,81}. An alternative interpretation is suggested by the co-existence of high charcoal abundance and illite minerals (Fig. 2), as the transformation of illite from smectite in soils has been shown to be activated by wildfire^{82–84}. This phenomenon could potentially also explain the co-occurrence of illite, CaCO_3 and macrocharcoal on a precessional time scale (Fig. 2). Both scenarios, either that of enhanced physical erosion or wildfire induced in situ transformation of clays, may have provided an input of illite during a more seasonal climate regime. Hence, increased fire activity appears to occur during a strongly seasonal climate phase forced by climatic shifts over precessional timescales (Fig. 3).

A similar mechanism has been proposed for precession driven wildfire activity in the Quaternary subtropics of South Africa²⁷. During a maximum in precessional forcing (austral summer in perihelion) the southern hemisphere experienced increased seasonality, and changes in insolation, shifting the ITCZ

southward. The hot summer experienced a strong monsoon, in which grasslands gathered biomass, whilst in the cooler and dry winter, the lowered fuel moisture allowed ignition of dry grasses and hence an increase in wildfire activity²⁷. Likewise, Zhang et al.²⁹ suggested that wildfires recorded in Middle Jurassic mires occurred during phases of high seasonal contrast. It appears that similarly linked climate and vegetation shifts operated in the Early Jurassic over precessional timescales, and that these also drove changes in wildfire activity. Indeed, it has been proposed that peaks in spore abundance (i.e. wet loving plants) in the Bristol Channel Basin are modulated by precession, where they are indicative of an enhanced hydrological cycle and abundant ferns⁶⁵.

In conclusion, we argue that fire activity is strongly influenced by orbital cycles over short (precessional) timescales, with our ~350 kyr record hinting at a modulation of the observed precession signal in the fire record by long eccentricity, based on the strongly evidenced shift in hydrology. We find that fire activity is greater when orbital changes led to extremes in seasonality (Fig. 3) and these changes in fire activity appear to be driven by the variations in the hydrological cycle, which influenced fuel load (vegetation biomass), ignition, and spread potential. It is expected that orbitally driven climate shifts also influenced the type of fuel by shifting the composition of ecosystems. Therefore, we suggest that high-resolution palynological studies will help to build further understanding between natural orbitally forced changes in climate and the composition of ecosystems on these timescales.

The findings of this research indicate that major shifts in fire activity were likely related to orbital forcing in the studied mid-latitude succession of the warm climate of the Early Jurassic. Quaternary records from low and mid-latitude locations indicate similarly that increased seasonality was linked to either a longer dry season (biomass not limited) or a more intense wet season (increasing biomass) leading to enhanced fire activity. These findings suggest that in these regions, orbital forcing influenced long-term fire activity in deep time, as well as in the Quaternary period. Therefore, orbital forcing likely plays an important role in determining fire regimes throughout Earth's history. Our results highlight that what could be considered relatively minor climatic shifts have a strong influence on wildfire activity, which helps put into perspective the apparent shifts in wildfire activity due to anthropogenic causes².

Materials and methods

Location and geology. In the Early Jurassic, the Cardigan Bay Basin was located at a mid-palaeolatitude of ~35°N⁸⁵, within the Laurasian Seaway^{86,87} (Fig. 1).

Mochras was situated south of the Viking Corridor that linked the north-western Tethys Ocean to the Boreal Sea⁸⁸. Hence, the Mochras location was subject to both polar and equatorial influences. In the SW, the Tethys Ocean was connected to the eastern Panthalassa via the Hispanic Corridor during the Early Jurassic^{89,90}.

The Mochras sediments were deposited within a basinal marine setting with influence from nearby terrigenous sources around the Cardigan Bay area^{49,91}. The Cardigan Bay Basin sedimentary fill was downthrown against the Early Paleozoic Welsh Massif by a major normal fault system, that may have comprised the Bala, Mochras and Tonfanau faults at the eastern and south-eastern margins of the basin in Late Paleozoic–Early Mesozoic time^{91–94}.

The Mochras borehole, formally 'Llanbedr (Mochras Farm)', was drilled onshore on the Cardigan Bay coast, North Wales (52°48'32"N, 4°08'44"W) between the years 1967–1969^{43,92,94,95}. Coring recovered a ~1300 m thick Early Jurassic sequence (601.83–1906.78 mbs), yielding a relatively complete and expanded Early Jurassic succession that is double the thickness of same age strata in other well-studied UK and European cores and outcrops^{43,46,95}. The Early Jurassic sequence is underlain by Triassic and unconformably overlain by Cenozoic and Quaternary successions⁹⁵. The relatively homogeneous lithology dominated by argillaceous sediments with alternating muddy limestones, marls and mudstones indicates a relatively open- and deep-marine (hemipelagic) setting⁸⁸.

The sections of the Mochras core are stored in cardboard core boxes at the British Geological Survey, Keyworth, Nottingham, UK, under ambient conditions. The Pliensbachian Stage in the Mochras borehole occurs between the depths of ~865 to ~1250 metres below surface (mbs). The interval in the core spanning the

Pliensbachian comprises mudstone and limestone alternations, with a persistent cyclicity at $\sim 1 \pm 0.5$ m wavelength⁴³. Intervals within the Pliensbachian are silty, locally sandy, and levels of relative organic enrichment occur throughout⁴⁶. Relatively continuous slabbed core in one-metre sections are preserved for the Pliensbachian and Toarcian part of Mochras⁹⁵. The strata from the Upper Pliensbachian (Margaritatus Zone), pre-dating the Late Pliensbachian cooling event, show clear lithological couplets of calcareous mudstone and organic matter enriched mudstone at the ~ 1 m scale⁴³.

This interval of the Upper Pliensbachian Subnodosus-Gibbosus subzones of the Margaritatus Zone, 934–951.3 mbs, was sampled at a high resolution of ~ 10 cm for palynological processing, clay mineralogy, bulk organic carbon isotope analysis, TOC and CaCO_3 . In total 151 cubes ($\sim 2 \times 2$ cm) were cut from the core sections or, where the correct depth was present in already cut and bagged sample from previous studies, this material has been used instead. All samples were split in half along the depth axis. One part of the sample was used for charcoal and palynofacies analysis and the other half for XRD and mass spectrometry.

XRD-analysis of clay minerals. Bulk-rock samples (~ 5 g) were first gently crushed and powdered by hand in an agate mortar. About 2–3 g of the powdered sample

was then decarbonated with a 0.2 M HCl solution. The clay sized fraction ($< 2 \mu\text{m}$) was extracted, smeared and oriented on glass slides and subsequently analysed by X-ray diffraction (XRD) using a Bruker D4 Endeavour diffractometer (Bruker, Billerica, MA, USA) with $\text{Cu K}\alpha$ radiations, LynxEye detector and Ni filter under 40 kV voltage and 25 mA intensity (Biogéosciences Laboratory, Université Bourgogne/Franche-Comté, Dijon). The clay phases were discriminated in three runs per sample: (1) air-drying at room temperature; (2) ethylene-glycol solvation during 24 h; (3) heating at 490 °C during 2 h, following Moore & Reynolds⁹⁶.

Clay minerals were identified using their main diffraction (d_{001}) peak and by comparing the three diffractograms obtained. The MACDIFF 4.2.5. software⁹⁷ was used to estimate the proportions of each clay mineral on glycolated diffractograms. The identification of the clay minerals further follows the methods in Deconinck et al.⁴⁹ and Moore & Reynolds⁹⁶.

XRF-Elemental analysis. High resolution (1 cm) elemental concentrations were obtained by automated X-ray fluorescence (XRF) analyses on the slabbed archive half of the Mochras core for the studied interval (934–951 mbs). XRF analyses were conducted with the ITRAX MC, with a 30 s measurement window. Long-term drift

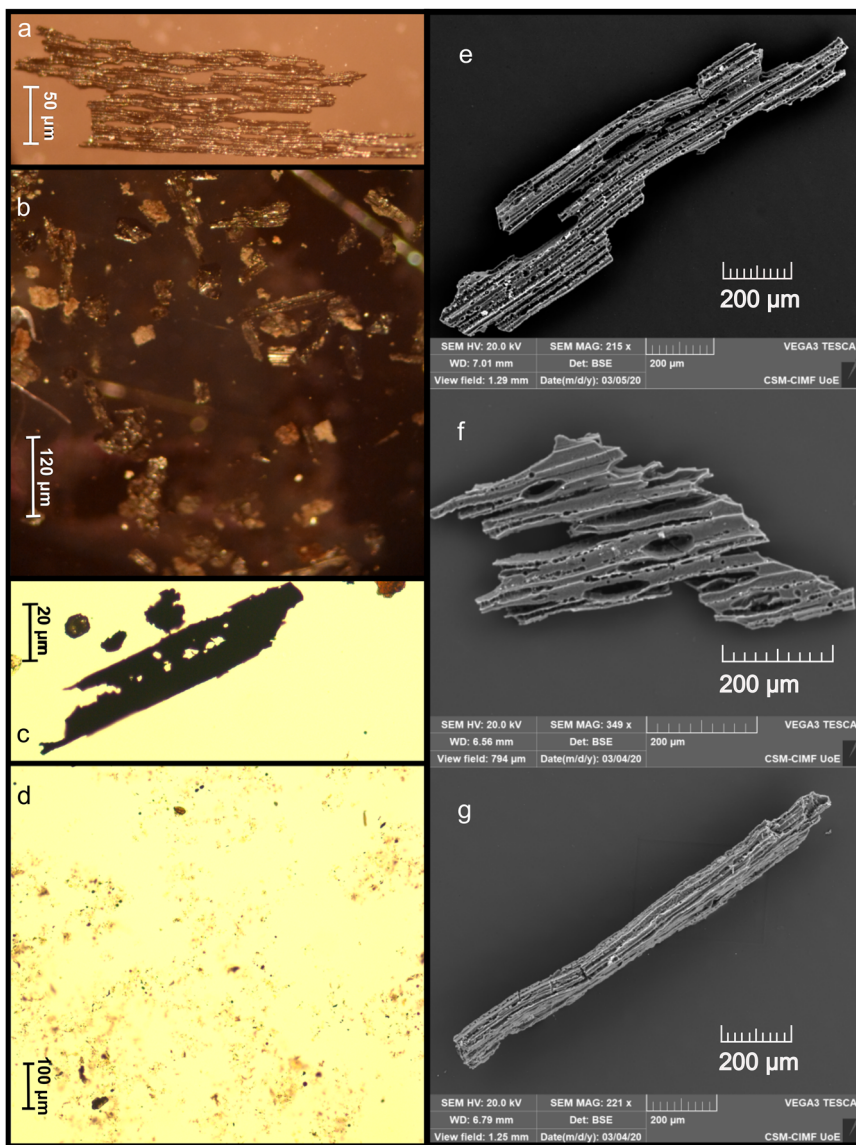


Fig. 5 Microscope images of macrocharcoal, microcharcoal and typical palynofacies of the studied interval of the Mochras borehole. **a** Macroscopic charcoal particle observed under the stereomicroscope. Identification characteristics are high reflection, brittle appearance, preserved anatomical structure and black in colour. **b** View of a typical macrocharcoal sample under the stereomicroscope. **c** Microscopic charcoal particle observed under an optical microscope, identification characteristics are opaqueness, black in colour, angular and lath-like morphology. **d** Typical palynofacies sample from the 934–951 mbs interval of the Mochras borehole. Abundant amorphous organic matter is present, with unstructured and structured terrestrial phytoclasts. **e–g** Scanning Electron Microscope (SEM) images of three macrocharcoal particles in the studied interval of the Mochras borehole. These charcoal particles show cellular structure, tracheids, bordering pits and rays.

in the measurement values was counteracted by regular internal calibration with a glass reference. Additionally, every 5 m, a 30 cm interval was duplicated.

TOC and bulk organic carbon isotope mass spectrometry. Part of the crushed samples for XRD-analysis was further powered in an agate mortar and taken for TOC (total organic carbon) and bulk organic carbon isotope analysis. These samples were decarbonized using 3.3% HCl. The samples were transferred to a hot bath of 79 °C for 1 h to remove siderite and dolomite. After the samples were centrifuged until neutral and oven dried, the material was crushed again and weighted in small tin capsules for mass spectrometry at the University of Exeter, Penryn Campus. A total of 149 samples have been analysed for TOC, CaCO₃ and $\delta^{13}\text{C}_{\text{org}}$.

Charcoal and palynofacies sample preparation. Between 10–25 g of sample was split into ~0.5 cm³ fragments, to minimize breakage of the particles and in order to extract charcoal and other organic matter using a palynological acid maceration technique. The samples were treated with cold hydrochloric acid (10% and 37% HCl) to remove carbonate. After this hydrofluoric acid (40% HF) was added to further remove silicates. After 48 h, cold concentrated HCl (37%) was added to avoid calcium fluoride precipitation. After neutralizing, 5 droplets of the mixed residue were taken for the analysis of palynofacies prior to any sieving. The remaining residue was sieved through a 125 µm mesh, and both fractions retained to separate the microscopic and macroscopic fraction of the charcoal, and the fine fraction sieved again at 10 µm, with the larger part of this retained.

Macroscopic charcoal (>125 µm) was counted using a Zeiss Stemi microscope (10 × 4 × magnification) with top lighting from a ‘goose necked’ light source. The entire >125 µm sieved residue sample was dispersed in a Petri dish filled with DI water and the number of charcoal particles present counted. The number of charcoal particles is expressed per 10 g of processed rock (n/g) in raw data format. If large unprocessed clusters of sediment were present in the sample, they were taken out and weighted after being dried. The dry weight of this unprocessed sediment aggregation has been deducted from the original sample weight. A total of 139 samples have been analysed for macroscopic charcoal.

A known quantity (125 µl) of the <125 µm but >10 µm of sieved residue was mounted onto microscope slides using glycerine jelly and glycerate liquid. Microscopic charcoal was counted using an Olympus (BX53) transmitted light microscope (40 × 10 × lens). Four transects (two transects in the middle and one on the left and right side of the coverslip) of each palynological slide were observed and the numbers of charcoal particles counted. These data were then scaled up to the known quantity of the sample⁹⁸. A total of 144 samples were analysed for microscopic charcoal.

Both size fractions of charcoals were identified according to the following criteria: opaque and black in colour, reflective of light, lustrous shine, often an elongated lath-like shape that shows sharp edges, original anatomy preserved, and fracture is brittle with splintery fragmentation⁹⁹ (Fig. 5).

Owing to the cyclic deposition of limestone and mudstone units throughout the section, we accounted for the effect of sediment dilution (dilution by biogenic or terrigenous material) in our charcoal quantifications. We normalised our macro and micro charcoal abundances with Ca (biogenic) and Si, Ti, Al and Fe (terrigenous) content gathered from the XRF trace element analyses, following a similar approach as Daniau et al.²⁷. We firstly assessed whether changes in the terrestrial influx (terrigenous) to the marine environment was driving any of the patterns we were seeing in the charcoal abundances. We normalised the ratios of the terrigenous elements (TE) to carbonate (Ca) ($\Sigma\text{TE}/\text{Ca}$) and subtracted the resulting percentage from the raw charcoal data. This effectively allowed us to express charcoal per gram of decarbonated sediment without any changes in terrestrial influx (Supplementary Fig. 4). Secondly, as this interval of the Jurassic is carbonate-rich, it could be that the charcoal and terrigenous element variations could be due to carbonate dilution.

Therefore, we further explored this normalised estimate for the charcoal without using Ca. A Pearson correlation ($r = >0.88$) indicated that Si has the highest R² to Al, Fe and Ti. As Si is most similar in pattern to Al, Fe and Ti, Si was used to ratio Fe, Ti, and Al against. These ratios have also been normalized and this percentage has been subtracted as a terrestrial influx number from the charcoal counts per 10 g. All these corrections, including and excluding Ca, are plotted in Supplementary Fig. 4. All normalised charcoal abundance (micro and macro charcoal) retain the same pattern of variability as the unnormalized abundances. Indicating that the variations in charcoal abundances reflect alterations in fire activity rather than dilution or enhancement from biogenic or terrigenous material.

We also assessed the palynofacies to observe changes in the nature of the organic material in the different sedimentary units. Palynofacies types were quantified on a palynological slide using the optical light microscope (40 × 10 × magnification). A total of 132 samples have been analysed for palynofacies. The palynofacies were organized into groups broadly adopted from Oboh-Ikuenobe et al.⁵³ (see Supplementary Fig. 8). The terrestrial palynomorphs identified are embryophytic spores and pollen grains derived from land plants; i.e. sporomorphs. Fungal remains are grouped separately and are recognized by dark brown spores, filamentous hyphae and mycelia, but were extremely sparse in the studied samples. Marine palynomorphs group dinoflagellates, acritarchs, prasinophytes and foraminifera. Fresh water algae were not found in these samples. Next to the

palynomorphs, structured and unstructured phytoclasts form two groups. Structured phytoclasts are defined as structured remains of land plants, including lath-shaped or blocky wood particles, parenchyma and thin cuticle fragments. With the exception of black debris and charcoal, any fragments with some form of cellular structure or definite shape is included in this category. Unstructured phytoclasts include highly degraded plant remains with indistinct structure with colours ranging from yellow to dark brown and nearly black, dark brown debris, and amber-coloured, globular to angular particles of resin. Charcoal also forms a group, based on the same characteristics as the microcharcoal (angular, black, lath-like, original plant structure preserved). Black debris is defined by most particles that are opaque and often having shapes similar to wood, although some are rounded and appear to be highly oxidized palynomorphs. This group does not include pyrite framboids but does include palynomorphs that are filled in with pyrite, where the original family could not be recognized. Amorphous organic matter is described as fluffy, clotted and granular masses with colours ranging from almost colourless to yellow and pale brown. We considered this category to be marine in origin, where it formed as a result of degradation of algal matter.

Organic particles are counted in transects of the microscope slide up to ~300 particles. If samples are dominated by one type of organic material, counting was continued until at least 100 other organic particles were counted.

Statistical analyses. We used a Pearson correlation to test for possible correlation between the proxies and the significance using RMatlab2017b. The *p* value tests the hypothesis of no correlation against the alternative hypothesis of a positive or negative correlation, with the significance level at $p = 0.05$. See Supplementary Fig. 5.

Spectral analysis test for orbital cyclicity. Spectral and time-series analysis on the 934–951 mbs Mochras record of macrocharcoal, percentage illite, percentage terrestrial phytoclasts and CaCO₃ was aimed to test whether the visually observed lithological-scale fluctuations are paced by precession (~20 kyr) orbital parameters, and by comparison to the astrochronologically tuned Pliensbachian time-scale at Mochras. Data preparation and spectral and time-series analysis were performed using the program Acycle¹⁰⁰ for Matlab, version R2017b.

The proxy data-series were converted into a time series by tuning this interval to the ~100 kyr eccentricity cycle of the Ca record that exists for the Pliensbachian of Mochras⁴³. This dataset was originally tuned to the 405 kyr cycle by Ruhl et al.⁴³, but for this interval we tuned the Ca-record of the Margaritatus Zone (~920–1015 mbs) to the 100 kyr eccentricity peaks, creating 19 tie points (See Supplementary Fig. 1).

Using this age model, the power spectra were run in the time domain in the software Acycle¹⁰⁰ using the multi-taper method, time-bandwidth product 2 and the robust red noise model. The main periods (~17–20 kyr, ~21–27 kyr, ~30–50 kyr) observed in the CaCO₃, illite, charcoal and percentage terrestrial phytoclasts, indicate the presence of precession and obliquity in the assessed proxy records. Subsequently, the dominant spectral components of obliquity and precession were extracted with Gaussian filtering and compared to the raw datasets. Long term cycles (100 kyr and 405 kyr) were extracted from the Ca record of Ruhl et al.⁴³ spanning the Margaritatus Zone of the Pliensbachian stage.

Data availability

All raw data used in the research has been made available in the supplementary data file ‘Supplementary Data file 1’. This includes: Additional analyses in Supplementary Notes 1 to 6 and all the relevant data files to repeat this analysis. The Supplementary Data file 1 is available at the National Geoscience Data Centre at Keyworth (NGDC) at <https://doi.org/10.5285/d6b7c567-49f0-44c7-a94c-e82fa17f98e>. The full Mochras XRF dataset is in ref.¹⁰¹.

Received: 2 February 2021; Accepted: 26 October 2021;

Published online: 30 November 2021

References

1. Stocker, T. F. et al. *IPCC, 2013: Climate Change 2013: The Physical Science Basis. Contribution of Working Group I to the Fifth Assessment Report of the Intergovernmental Panel on Climate Change* (Cambridge Univ. Press, 2013).
2. Jones, M. W. et al. Climate change increases risk of wildfires. *ScienceBrief Review* **116**, 117 (2020).
3. Rogers, B. M., Balch, J. K., Goetz, S. J., Lehmann, C. E. & Turetsky, M. Focus on changing fire regimes: interactions with climate, ecosystems, and society. *Environmental Research Letters* **15**, 030201 (2020).
4. Archibald, S., Lehmann, C. E., Gómez-Dans, J. L. & Bradstock, R. A. Defining pyromes and global syndromes of fire regimes. *Proceedings of the National Acadam of Science* **110**, 6442–6447 (2013).

5. Donovan, G. H. & Brown, T. C. Be careful what you wish for: the legacy of Smokey Bear. *Frontiers in Ecology and the Environment* **5**, 73–79 (2007).
6. Ghil, M. Natural climate variability. *Encyclopedia Global Environmental Change* **1**, 544–549 (2002).
7. Hinnov, L. A. Cyclostratigraphy and its revolutionizing applications in the earth and planetary sciences. *Geological Society of America Bulletin* **125**, 1703–1734 (2013).
8. Lantink, M. L., Davies, J. H., Mason, P. R., Schaltegger, U. & Hilgen, F. J. Climate control on banded iron formations linked to orbital eccentricity. *Nature Geoscience* **12**, 369–374 (2019).
9. Berger, A. Milankovitch theory and climate. *Reviews of Geophysics* **26**, 624–657 (1988).
10. Laskar, J. Astrochronology in *Geological Time Scale 2020* (eds Gradstein, F. M., Ogg, J. G., Schmitz, M. D. & Ogg, G. M.) 139–158 (Elsevier, 2020).
11. Shackleton, N. J. & Pisias, S. N. Atmospheric carbon dioxide, orbital forcing, and climate. *The Carbon Cycle and Atmospheric CO₂: Natural Variations Archean to Present, Geophysics Monograph Series* **32**, 303–317 (1985).
12. Huybers, P. & Wunsch, C. Obliquity pacing of the late Pleistocene glacial terminations. *Nature* **434**, 491–494 (2005).
13. Kutzbach, J. E., Liu, X., Liu, Z. & Chen, G. Simulation of the evolutionary response of global summer monsoons to orbital forcing over the past 280,000 years. *Climate Dynamics* **30**, 567–579 (2008).
14. Weedon, G. P. Hemipelagic shelf sedimentation and climatic cycles: the basal Jurassic (Blue Lias) of South Britain. *Earth and Planetary Science Letters* **76**, 321–335 (1986).
15. Weedon, G. P., Jenkyns, H. C., Coe, A. L. & Hesselbo, S. P. Astronomical calibration of the Jurassic time-scale from cyclostratigraphy in British mudrock formations. *Philosophical Transactions of the Royal Society of London. Series A: Mathematical, Physical and Engineering Sciences* **357**, 1787–1813 (1999).
16. Van Buchem, F. S. P., McCave, I. N. & Weedon, G. P. Orbitally induced small-scale cyclicity in a siliciclastic epicontinental setting (Lower Lias, Yorkshire, UK) in *Orbital forcing and cyclic sequences*, Special Publication of the International Association of Sedimentologists (eds de Boer, P. L. & Smith, D. G.) 345–366 (1994).
17. Zachos, J. C., McCarren, H., Murphy, B., Röhl, U. & Westerhold, T. Tempo and scale of late Paleocene and early Eocene carbon isotope cycles: Implications for the origin of hyperthermals. *Earth and Planetary Science Letters* **299**, 242–249 (2010).
18. Martinez, M. & Dera, G. Orbital pacing of carbon fluxes by a ~9-My eccentricity cycle during the Mesozoic. *Proceedings of the National Academy of Sciences* **112**, 12604–12609 (2015).
19. Laskar, J. The chaotic motion of the solar system: a numerical estimate of the size of the chaotic zones. *Icarus* **88**, 266–291 (1990).
20. Varadi, F., Runnegar, B. & Ghil, M. Successive refinements in long-term integrations of planetary orbits. *The Astrophysical Journal* **592**, 620 (2003).
21. Laskar, J. et al. Long term evolution and chaotic diffusion of the insolation quantities of Mars. *Icarus* **170**, 343–364 (2004).
22. Imbrie, J. & Imbrie, K. P. *Ice ages: solving the mystery* (Harvard University Press, 1979).
23. Berger, A. & Loutre, M. F. Climate 400,000 years ago, a key to the future? *Geophysical Monograph Series* **137**, 17–26 (2003).
24. Laskar, J., Fienga, A., Gastineau, M. & Manche, H. La2010: a new orbital solution for the long-term motion of the Earth. *Astronomy & Astrophysics* **532**, A89 (2011).
25. Verardo, D. J. & Ruddiman, W. F. Late Pleistocene charcoal in tropical Atlantic deep-sea sediments: climatic and geochemical significance. *Geology* **24**, 855–857 (1996).
26. Thevenon, F., Bard, E., Williamson, D. & Beaufort, L. A biomass burning record from the West Equatorial Pacific over the last 360 ky: methodological, climatic and anthropic implications. *Palaeogeography, Palaeoclimatology, Palaeoecology* **213**, 83–99 (2004).
27. Daniau, A. L. et al. Orbital-scale climate forcing of grassland burning in southern Africa. *Proceedings of the National Academy of Sciences* **110**, 5069–5073 (2013).
28. Inoue, J., Okuyama, C. & Takemura, K. Long-term fire activity under the East Asian monsoon responding to spring insolation, vegetation type, global climate, and human impact inferred from charcoal records in Lake Biwa sediments in central Japan. *Quaternary Science Reviews* **179**, 59–68 (2018).
29. Zhang, Z. et al. Precession-scale climate forcing of peatland wildfires during the early middle Jurassic greenhouse period. *Global and Planetary Change* **184**, 103051 (2020).
30. Shi, Y. et al. Wildfire evolution and response to climate change in the Yinchuan Basin during the past 1.5 Ma based on the charcoal records of the PL02 core. *Quaternary Science Reviews* **241**, 106393 (2020).
31. Martínez-Abarca, L. R. et al. Environmental changes during MIS6-3 in the Basin of Mexico: a record of fire, lake productivity history and vegetation. *J. South American Earth Sciences* **109**, 103231 (2021).
32. Whitlock, C. & Larsen, C. Charcoal as a fire proxy in *Tracking environmental change using lake sediments* (eds Smol, J. P., Birks, H. J. B., Last, W. M., Bradley, R. S. & Alverson, K.) 75–97 (Springer, Dordrecht, 2002).
33. Hao, Y., Han, Y., An, Z. & Burr, G. S. Climatic control of orbital time-scale wildfire occurrences since the late MIS 3 at Qinghai Lake, monsoon marginal zone. *Quaternary International* **550**, 20–26 (2020).
34. Zhou, B. et al. Elemental carbon record of paleofire history on the Chinese Loess Plateau during the last 420 ka and its response to environmental and climate changes. *Palaeogeography, Palaeoclimatology, Palaeoecology* **252**, 617–625 (2007).
35. Kappenberg, A., Lehndorff, E., Pickarski, N., Litt, T. & Amelung, W. Solar controls of fire events during the past 600,000 years. *Quaternary Science Reviews* **208**, 97–104 (2019).
36. Han, Y. et al. Asian inland wildfires driven by glacial–interglacial climate change. *Proceedings of the National Academy of Sciences* **117**, 5184–5189 (2020).
37. Scott, A. C. & Glasspool, I. J. Observations and experiments on the origin and formation of inertinite group macerals. *International Journal of Coal Geology* **70**, 53–66 (2007).
38. House, M. R. A new approach to an absolute timescale from measurements of orbital cycles and sedimentary microrhythms. *Nature* **315**, 721–725 (1985).
39. Hesselbo, S. P. & Jenkyns, H. C. A comparison of the Hettangian to Bajocian successions of Dorset and Yorkshire. *Field Geology of the British Jurassic*, Geological Society of London (1995).
40. Weedon, G. P. & Jenkyns, H. C. Cyclostratigraphy and the Early Jurassic timescale: data from the Belemnite Marls, Dorset, southern England. *Geological Society of America Bulletin* **111**, 1823–1840 (1999).
41. Ruhl, M. et al. Astronomical constraints on the duration of the early Jurassic Hettangian stage and recovery rates following the end-Triassic mass extinction (St Audrie's Bay/East Quantoxhead, UK). *Earth and Planetary Science Letters* **295**, 262–276 (2010).
42. Hüsing, S. K. et al. Astronomically-calibrated magnetostratigraphy of the lower Jurassic marine successions at St. Audrie's Bay and East Quantoxhead (Hettangian–Sinemurian; Somerset, UK). *Palaeogeography, Palaeoclimatology, Palaeoecology* **403**, 43–56 (2014).
43. Ruhl, M. et al. Astronomical constraints on the duration of the Early Jurassic Pliensbachian Stage and global climatic fluctuations. *Earth and Planetary Science Letters* **455**, 149–165 (2016).
44. Xu, W., Ruhl, M., Hesselbo, S. P., Riding, J. B. & Jenkyns, H. C. Orbital pacing of the Early Jurassic carbon cycle, black-shale formation and seabed methane seepage. *Sedimentology* **64**, 127–149 (2017).
45. Hinnov, L. A., Ruhl, M. R. & Hesselbo, S. P. Reply to the Comment on “Astronomical constraints on the duration of the Early Jurassic Pliensbachian Stage and global climatic fluctuations” (Ruhl et al. *Earth and Planetary Science Letters*, 455 149–165). *Earth and Planetary Science Letters* **481**, 415–419 (2018).
46. Storm, M. S. et al. Orbital pacing and secular evolution of the Early Jurassic carbon cycle. *Proceedings National Academy Science* **117**, 3974–3982 (2020).
47. Ogg, J. G., Hinnov, L. A. & Huang, C. Jurassic in *The geologic time scale* (eds Gradstein, F. M., Ogg, J. G., Schmitz, M. D. & Ogg, G. M.) 731–791 (Elsevier, 2012).
48. Hinnov, L. A. & Hilgen, F. J. Cyclostratigraphy and astrochronology in *The Geologic Time Scale 2012* (eds Gradstein, F. M., Ogg, J. G., Schmitz, M. D. & Ogg, G. M.) 63–83 (2012).
49. Deconinck, J. F., Hesselbo, S. P. & Pellenard, P. Climatic and sea-level control of Jurassic (Pliensbachian) clay mineral sedimentation in the Cardigan Bay Basin, Llanbedr (Mochras Farm) borehole, Wales. *Sedimentology* **66**, 2769–2783 (2019).
50. Chamley, H. *Clay sedimentology* 623 (Springer, Berlin, Heidelberg, 1989).
51. Ruffell, A., McKinley, J. M. & Worden, R. H. Comparison of clay mineral stratigraphy to other proxy palaeoclimate indicators in the Mesozoic of NW Europe. *Philosophical Transactions of the Royal Society London A: Mathematical, Physical and Engineering Sciences* **360**, 675–693 (2002).
52. Ghosh, S., Mukhopadhyay, J. & Chakraborty, A. Clay mineral and geochemical proxies for intense climate change in the permian gondwana rock record from eastern india. *Research*, 8974075 (2019).
53. Oboh-Ikuenobe, F. E., Obi, C. G. & Jaramillo, C. A. Lithofacies, palynofacies, and sequence stratigraphy of Palaeogene strata in Southeastern Nigeria. *Journal of African Earth Sciences* **41**, 79–101 (2005).
54. Sprovieri, M. et al. Late Cretaceous orbitally-paced carbon isotope stratigraphy from the Bottaccione Gorge (Italy). *Palaeogeography, Palaeoclimatology, Palaeoecology* **379**, 81–94 (2013).
55. Raucsik, B. & Varga, A. Climato-environmental controls on clay mineralogy of the Hettangian–Bajocian successions of the Mecsek Mountains, Hungary: an evidence for extreme continental weathering during the early Toarcian oceanic anoxic event. *Palaeogeography, Palaeoclimatology, Palaeoecology* **265**, 1–13 (2008).

56. Martinez, M. Mechanisms of preservation of the eccentricity and longer-term Milankovitch cycles in detrital supply and carbonate production in hemipelagic marl-limestone alternations. *Stratigraphy & Timescales* **3**, 189–218 (2018).
57. Cochrane, M. A. & Ryan, K. C. Fire and fire ecology: Concepts and principles in *Tropical fire ecology*, 25–62 (2009).
58. Belcher, C. M. & Hudspeth, V. A. The formation of charcoal reflectance and its potential use in post-fire assessments. *International Journal of Wildland Fire* **25**, 775–779 (2016).
59. Archibald, S. et al. Biological and geophysical feedbacks with fire in the Earth system. *Environmental Research Letters* **13**, 033003 (2018).
60. Van de Schootbrugge, B. et al. Early Jurassic climate change and the radiation of organic-walled phytoplankton in the Tethys Ocean. *Paleobiology* **31**, 73–97 (2005).
61. Vakhrameyev, V. A. Classopollis pollen as an indicator of Jurassic and Cretaceous climate. *International Geology Review* **24**, 1190–1196 (1982).
62. Belcher, C. M., Collinson, M. E. & Scott, A. C. A 450-Million-Year History of Fire in *Fire phenomena and the earth system* (ed. Belcher, C. M.) 229–249 (Wiley-Blackwell, 2013).
63. Rees, P. M., Ziegler, A. M. & Valdes, P. J. Jurassic phytogeography and climates: new data and model comparisons in *Warm climates in earth history* (eds Huber, B. T., Macleod, K. G. & Wing, S. L.) 297–318 (2000).
64. Dera, G. et al. Distribution of clay minerals in Early Jurassic Peritethyan seas: palaeoclimatic significance inferred from multiproxy comparisons. *Palaeogeography, Palaeoclimatology, Palaeoecology* **271**, 39–51 (2009).
65. Bonis, N. R., Ruhl, M. & Kürschner, W. M. Milankovitch-scale palynological turnover across the Triassic–Jurassic transition at St. Audrie's Bay, SW UK. *Journal of the Geological Society* **167**, 877–888 (2010).
66. Deconinck, J. F. et al. Diagenetic and environmental control of the clay mineralogy, organic matter and stable isotopes (C, O) of Jurassic (Pliensbachian–lowermost Toarcian) sediments of the Rodiles section (Asturian Basin, Northern Spain). *Marine and Petroleum Geology* **115**, 104286 (2020).
67. Dewhurst, R. A., Smirnov, N. & Belcher, C. M. Pine Species That Support Crown Fire Regimes Have Lower Leaf-Level Terpene Contents Than Those Native to Surface Fire Regimes. *Fire* **3**, 17 (2020).
68. Berger, A., Loutre, M. F. & Dehant, V. Astronomical frequencies for pre-Quaternary palaeoclimate studies. *Terra Nova* **1**, 474–479 (1989).
69. House, M. R. & Gale, A. S. (eds). *Orbital forcing timescales and cyclostratigraphy*, 85, 1–18 (Geological Society, 1995).
70. James, N. P. Facies models 7. Introduction to carbonate facies models. *Geoscience Canada* **4**, 123–125 (1977).
71. Nelson, C. S., Keane, S. L. & Head, P. S. Non-tropical carbonate deposits on the modern New Zealand shelf. *Sedimentary Geology* **60**, 71–94 (1988).
72. Chave, K. E. Recent carbonate sediments—an unconventional view. *Journal of Geological Education* **15**, 200–204 (1967).
73. Parrish, J. T. & Curtis, R. L. Atmospheric circulation, upwelling, and organic-rich rocks in the Mesozoic and Cenozoic eras. *Palaeogeography, Palaeoclimatology, Palaeoecology* **40**, 31–66 (1982).
74. Crowley, T. J., Baum, S. K. & Hyde, W. T. Milankovitch fluctuations on supercontinents. *Geophysical research letters* **19**, 793–796 (1992).
75. Parrish, J. T. Climate of the supercontinent Pangea. *The J. Geology* **101**, 215–233 (1993).
76. Kutzbach, J. E. & Gallimore, R. G. Pangaeian climates: megamonsoons of the megacontinent. *Journal of Geophysical Research: Atmospheres* **94**, 3341–3357 (1989).
77. Kutzbach, J. E. Idealized Pangaeian climates: sensitivity to orbital change. Pangea; paleoclimate, tectonics, and sedimentation during accretion, zenith and breakup of a supercontinent. *Geological Society of America* **15**, 41–55 (1994).
78. Sellwood, B. W. & Valdes, P. J. Mesozoic climates: General circulation models and the rock record. *Sedimentary geology* **190**, 269–287 (2006).
79. Mutti, M. & Hallock, P. Carbonate systems along nutrient and temperature gradients: some sedimentological and geochemical constraints. *International Journal of Earth Sciences* **92**, 465–475 (2003).
80. Clift, P. D., Wan, S. & Blusztajn, J. Reconstructing chemical weathering, physical erosion and monsoon intensity since 25 Ma in the northern South China Sea: a review of competing proxies. *Earth-Science Reviews* **130**, 86–102 (2014).
81. Clift, P. D. et al. Chemical weathering and erosion responses to changing monsoon climate in the Late Miocene of Southwest Asia. *Geological Magazine* **157**, 939–955 (2020).
82. Arocena, J. M. & Opio, C. Prescribed fire-induced changes in properties of sub-boreal forest soils. *Geoderma* **113**, 1–16 (2003).
83. Certini, G. Effects of fire on properties of forest soils: a review. *Oecologia* **143**, 1–10 (2005).
84. Reynard-Callanan, J. R., Pope, G. A., Gorrington, M. L. & Feng, H. Effects of high-intensity forest fires on soil clay mineralogy. *Physical Geography* **31**, 407–422 (2010).
85. Torsvik, T. & Cocks, L. Jurassic in *Earth History and Palaeogeography* 208–218 (Cambridge University Press, 2016).
86. Bjerrum, C. J., Surlyk, F., Callomon, J. H. & Slingerland, R. L. Numerical paleoceanographic study of the Early Jurassic transcontinental Laurasian Seaway. *Paleoceanography* **16**, 390–404 (2001).
87. Hesselbo, S. P. & Pieńkowski, G. Stepwise atmospheric carbon-isotope excursion during the Toarcian oceanic anoxic event (Early Jurassic, Polish Basin). *Earth and Planetary Science Letters* **301**, 365–372 (2011).
88. Sellwood, B. W. & Jenkyns, H. G. Basins and swells and the evolution of an epeiric sea: (Pliensbachian–Bajocian of Great Britain). *Journal of the Geological Society* **131**, 373–388 (1975).
89. Damborenea, S. E., Echevarría, J. & Ros-Franch, S. *Southern hemisphere palaeobiogeography of Triassic–Jurassic marine bivalves*. (Springer, 2012).
90. Korte, C. et al. Jurassic climate mode governed by ocean gateway. *Nature Communications* **6**, 1–7 (2015).
91. Dobson, M. R. & Whittington, R. J. The geology of Cardigan Bay. *Proceedings of the Geologists' Association* **98**, 331–353 (1987).
92. Woodland, A. W. *The Llanbedr (Mochras Farm) Borehole* Rep. No. 71/18 (Ed. Woodland, A. W.) 115 (Institute of Geological Sciences, 1971).
93. Tappin, D. R. et al. The Geology of Cardigan Bay and the Bristol Channel. United Kingdom offshore regional report, British Geological Survey, HMSO, 107 (1994).
94. Xu, W. et al. Evolution of the Toarcian (Early Jurassic) carbon-cycle and global climatic controls on local sedimentary processes (Cardigan Bay Basin, UK). *Earth and Planetary Science Letters* **484**, 396–411 (2018).
95. Hesselbo, S. P. et al. Mochras borehole revisited: A new global standard for Early Jurassic earth history. *Scientific Drilling* **16**, 81–91 (2013).
96. Moore, D. M. & Reynolds Jr, R. C. X-ray Diffraction and the Identification and Analysis of Clay Minerals (Oxford University Press, 1997).
97. Petschick, R. MacDiff 4.1. 2. Powder diffraction software (2000). Available from the author at <http://www.geol.uni-erlangen.de/html/software/Macdiff.html>.
98. Belcher, C. M., Collinson, M. E. & Scott, A. C. Constraints on the thermal energy released from the Chicxulub impactor: new evidence from multi-method charcoal analysis. *Journal of the Geological Society* **162**, 591–602 (2005).
99. Scott, A. C. Charcoal recognition, taphonomy and uses in palaeoenvironmental analysis. *Palaeogeography, Palaeoclimatology, Palaeoecology* **291**, 11–39 (2010).
100. Li, M., Hinnov, L. & Kump, L. A cycle: Time-series analysis software for paleoclimate research and education. *Computers & Geosciences* **127**, 12–22 (2019).
101. Damaschke, M., Wylde, S., Jiang, M., Hollaar, T. & Ullmann, C. V. LLANBEDR (MOCHRAS FARM) Core Scanning Dataset. NERC EDS National Geoscience Data Centre. (Dataset). <https://doi.org/10.5285/c09e9908-6a21-43a8-bc5a-944f9eb8b97e> (2021).

Acknowledgements

This is a contribution to the JET project funded by the Natural Environment Research Council (NERC) (grant number NE/N018508/1). SPH, CMB, JFD, MR and TPH, acknowledge funding from the International Continental Scientific Drilling Program (ICDP) and TPH acknowledges funding from the University of Exeter. SJB acknowledges previous funding from NERC (NE/L501669/1) that provided the proof of concept data for this study. We thank the British Geological Survey (BGS), especially James Riding, Scott Renshaw and Tracey Gallagher for facilitating access to the Mochras core over an extended period. Magret Damaschke and Simon Wylde are thanked for performing XRF scanning and for facilitating access to the Core Scanning Facility. Also, Clemens Ullmann and Mengjie Jiang are thanked for their help in the Core Scanning Facility. Magret Damaschke and Charles Gowing are thanked for discussion on the XRF-elemental results. We further thank Chris Mitchell and Clemens Ullmann for help with TOC and $\delta^{13}\text{C}_{\text{org}}$ analyses. Mark Grosvenor is thanked for his assistance with HF processing. Members of the JET team and FJ Hilgen are thanked for discussions on the Mochras record.

Author contributions

C.M.B. and T.P.H. conceived the study with input from S.P.H. S.J.B. produced a preliminary dataset that provided proof of concept for this study. M.R. advised T.P.H. and S.J.B. on the relevant sampling interval of the Mochras core. T.P.H. collected all rock samples from the Mochras core stored at the BGS. T.P.H. prepared the samples for charcoal identification, palynofacies, and bulk carbon isotope analysis. J.F.D. and T.P.H. processed clay mineralogical samples. T.P.H. analysed the samples and the data. L.M. advised and assisted T.P.H. with the palynofacies analysis, M.R. with the cyclostratigraphy and J.F.D. with the clay mineralogy. All authors contributed to discussing the results. T.P.H. wrote the manuscript with feedback and contributions from all authors.

Competing interests

The authors declare no competing interests.

Additional information

Supplementary information The online version contains supplementary material available at <https://doi.org/10.1038/s43247-021-00307-3>.

Correspondence and requests for materials should be addressed to Teuntje P. Hollaar.

Peer review information *Communications Earth & Environment* thanks the anonymous reviewers for their contribution to the peer review of this work. Primary Handling Editors: Ola Kwiecien and Clare Davis.

Reprints and permission information is available at <http://www.nature.com/reprints>

Publisher's note Springer Nature remains neutral with regard to jurisdictional claims in published maps and institutional affiliations.



Open Access This article is licensed under a Creative Commons Attribution 4.0 International License, which permits use, sharing, adaptation, distribution and reproduction in any medium or format, as long as you give appropriate credit to the original author(s) and the source, provide a link to the Creative Commons license, and indicate if changes were made. The images or other third party material in this article are included in the article's Creative Commons license, unless indicated otherwise in a credit line to the material. If material is not included in the article's Creative Commons license and your intended use is not permitted by statutory regulation or exceeds the permitted use, you will need to obtain permission directly from the copyright holder. To view a copy of this license, visit <http://creativecommons.org/licenses/by/4.0/>.

© The Author(s) 2021